Multi-Sensor Seismic Processing Approach using Geophones and HWC DAS in the Monitoring of CO2 Storage at the Hellisheiði Geothermal Field in Iceland

Bellezza, Cinzia; Barison, Erika; Farina, Biancamaria; Poletto, Flavio; Meneghini, Fabio; Böhm, Gualtiero; Draganov, Deyan; Janssen, Martijn T. G.; van Otten, Gijs; More Authors

DOI
10.3390/su16020877

Publication date
2024

Document Version
Final published version

Published in
Sustainability

Citation (APA)
Bellezza, C., Barison, E., Farina, B., Poletto, F., Meneghini, F., Böhm, G., Draganov, D., Janssen, M. T. G., van Otten, G., & More Authors (2024). Multi-Sensor Seismic Processing Approach using Geophones and HWC DAS in the Monitoring of CO2 Storage at the Hellisheiði Geothermal Field in Iceland. *Sustainability*, *16*(2), Article 877. https://doi.org/10.3390/su16020877

sustainability

MDPI

Article

Multi-Sensor Seismic Processing Approach using Geophones and HWC DAS in the Monitoring of CO_2 Storage at the Hellisheiði Geothermal Field in Iceland

Cinzia Bellezza [1,*], Erika Barison [1], Biancamaria Farina [1], Flavio Poletto [1], Fabio Meneghini [1], Gualtiero Böhm [1], Deyan Draganov [2], Martijn T. G. Janssen [2], Gijs van Otten [3], Anna L. Stork [4], Athena Chalari [4], Andrea Schleifer [1] and Sevket Durucan [5]

[1] OGS National Institute of Oceanography and Applied Geophysics, Borgo Grotta Gigante 42/c, Sgonico, 34010 Trieste, Italy; ebarison@ogs.it (E.B.)
[2] Department of Geosciences & Engineering, TU Delft, Stevinweg 1, 2628 CN Delft, The Netherlands; d.s.draganov@tudelft.nl (D.D.); mjanssen2@outlook.com (M.T.G.J.)
[3] Seismic Mechatronics, Habraken 2150, 5507 TH Veldhoven, The Netherlands; g.van.otten@seismic-mechatronics.com
[4] Silixa Ltd., 230 Centennial Park, Centennial Avenue, Elstree WD6 3SN, UK; anna.stork@silixa.com (A.L.S.); athena.chalari@silixa.com (A.C.)
[5] Department of Earth Science and Engineering, Royal School of Mines, Imperial College London, South Kensington Campus, London SW7 2AZ, UK
* Correspondence: cbellezza@ogs.it

Abstract: Geothermal power production may result in significant CO_2 emissions as part of the produced steam. CO_2 capture, utilisation, subsurface storage (CCUS) and developments to exploit geothermal resources are focal points for future clean and renewable energy strategies. The Synergetic Utilisation of CO_2 Storage Coupled with Geothermal Energy Deployment (SUCCEED) project aims to demonstrate the feasibility of using produced CO_2 for re-injection in the geothermal field to improve geothermal performance, while also storing the CO_2 as an action for climate change mitigation. Our study has the aim to develop innovative reservoir-monitoring technologies via active-source seismic data acquisition using a novel electric seismic vibrator source and permanently installed helically wound cable (HWC) fibre-optic distributed acoustic sensing (DAS) system. Implemented together with auxiliary multi-component (3C and 2C) geophone receiver arrays, this approach gave us the opportunity to compare and cross-validate the results using wavefields from different acquisition systems. We present the results of the baseline survey of a time-lapse monitoring project at the Hellisheiði geothermal field in Iceland. We perform tomographic inversion and multichannel seismic processing to investigate both the shallower and the deeper basaltic rocks targets. The wavefield analysis is supported by seismic modelling. The HWC DAS and the geophone-stacked sections show good consistency, highlighting the same reflection zones. The comparison of the new DAS technology with the well-known standard geophone acquisition proves the effectiveness and reliability of using broadside sensitivity HWC DAS in surface monitoring applications.

Keywords: CO_2 injection monitoring; geothermal reservoir; CCUS; surface seismic processing; distributed acoustic sensing (DAS); geophones

Citation: Bellezza, C.; Barison, E.; Farina, B.; Poletto, F.; Meneghini, F.; Böhm, G.; Draganov, D.; Janssen, M.T.G.; van Otten, G.; Stork, A.L.; et al. Multi-Sensor Seismic Processing Approach using Geophones and HWC DAS in the Monitoring of CO_2 Storage at the Hellisheiði Geothermal Field in Iceland. *Sustainability* **2024**, *16*, 877. https://doi.org/10.3390/su16020877

Academic Editors: Luisa F. Cabeza, Kazbulat Shogenov and Alla Shogenova

Received: 28 September 2023
Revised: 25 December 2023
Accepted: 9 January 2024
Published: 19 January 2024

1. Introduction

Geothermal energy derives from the Earth's core and it is stored in rocks and fluids in the subsurface. Natural displays of geothermal energy are volcanoes, fumaroles and geysers. Generation of electricity from geothermal power dates back to the beginning of the 20th century. Electricity production started at Larderello, Italy, in 1904 with an

experimental 10 kWe generator. In 2020, the electricity production worldwide had reached 95,098 GWh. For an historical overview and future scenarios of the use of geothermal energy, see [1]. Although geothermal energy is generally considered a clean energy source in terms of environmental impact, large-capacity geothermal power plants may emit significant amounts of CO_2 as part of the produced steam. Carbon capture, utilisation and underground storage (CCUS) and developments for the utilisation of geothermal resources are focal points for the future clean and renewable energy strategies. The main objectives of the SUCCEED project [2] are to explore and demonstrate the feasibility of utilising produced CO_2 for re-injection to enhance geothermal performance, while also storing the CO_2 as an action for climate change mitigation. The studies have been carried out in two existing facilities, at Kizildere in Turkey [3] and Hellisheiði in Iceland, that present a uniquely active geology and natural conditions suitable for geothermal energy production. This multidisciplinary project includes geochemical, geomechanical and geophysical studies, fluid flow modelling, as well as the development and use of innovative seismic monitoring techniques and hardware tools (including an electric seismic vibrator and DAS systems) for CCUS purposes. This study, focused on the Hellisheiði geothermal field, includes laboratory analysis [4] and field monitoring campaigns and describes the processing results.

More than ten years ago, the CarbFix Pilot Project [5,6] tested the feasibility of in situ mineral carbonation in basaltic rocks as a way to permanently and safely store CO_2 [7,8]. The CO_2 was captured from the Hellisheiði geothermal power plant and injected, dissolved in water, at the CarbFix pilot injection site. The verification of CO_2 mineralisation in the subsurface was achieved by tagging the injected CO_2 with radiocarbon (^{14}C) and using SF_5CF_3 and amidorhodamine G as conservative tracers to monitor the transport of the injected CO_2-charged water [9]. Details about the geothermal power plant and the projects performed over the years can be found in the literature (e.g., [10–13]). In the framework of the SUCCEED project, active and passive seismic approaches were used as complementary tools to investigate the behaviour of the injected CO_2 in geothermal reservoirs [14], with helically wound cable (HWC) distributed acoustic sensing (DAS) as seismic sensors. For this purpose, it is important to have high-resolution images of the subsurface. Often, a limiting factor for this is the requirement to have a sufficiently dense deployment of seismic sources and receivers at the surface and/or boreholes. The new developments in recent years of fibre-optic sensing of acoustic and seismic wavefields address the challenge of sufficiently dense receiver sampling. The DAS technology offers dense spatial and temporal sampling, less than 1 m and up to 100 kHz, respectively; measurements can be made on a single cable up to tens of km long. Another advantage of the fibre-optic technology over traditional seismic instruments (geophones) is that cables with polyimide coatings enable DAS measurements in high temperatures up to 300 °C, as often experienced in geothermal environments [2]. Fibre-optic sensing cables have been shown to be suitably robust for extended duration installations in geothermal fields [15], making them ideal to test and assess monitoring techniques at the Hellisheiði geothermal field to improve the long-term repeatable monitoring with a permanent installation.

Passive monitoring of geothermal reservoirs is widely used. In fact, microseismic, local, regional and teleseismic events can all provide useful information about a geothermal area on various scales (e.g., [16]). In recent years, passive monitoring of geothermal fields utilising linear and HWC fibre-optic DAS, deployed at the surface, has been analysed [14]. Recently, some authors used vertically installed fibre-optic cable in a geothermal injection well to record strain rates and detect earthquakes for monitoring purposes [17]. Standard DAS cables are not optimal for surface seismic acquisitions. In fact, a standard DAS has its highest sensitivity to P-waves when the angle of incidence ϑ of the wave is 0 degrees. The sensitivity decreases as $cos^2(\vartheta)$ as the angle of incidence increases, reaching its minimum when the wave propagation is orthogonal to the fibre (e.g., [18]). The broadside sensitivity of HWC is significantly improved with the angle of

incidence of a P-wave [19–21]. The use of HWC DAS for monitoring purposes in geothermal areas using an active source is still a topic under investigation, with the aim to understand its sensitivity to the different wavefields that can be recorded in a complex environment. Understanding the HWC DAS signals response could be of relevant importance for the development of a monitoring system in geothermal areas.

We present the results of the active-source seismic data acquisition performed at Hellisheiði and of the processing of the surface seismic monitoring data. The signals were generated by a novel electric seismic vibrator source (E-Vibe) and recorded using permanently installed HWC fibre-optic DAS, together with auxiliary multi-component geophone receiver arrays, the latter being used to validate the signals from the HWC DAS. This multi-receiver configuration was used for the baseline campaign (conducted in July 2021) of the planned time-lapse monitoring project. The integration of datasets from different types of sensors resulted in improved quality control (QC) performance and confirmed the consistency of the collected data [21]. The subsequent analysis compares the signal-to-noise ratio (S/N) and the sensitivity in the broadside HWC DAS measurements with the prediction and recognition of multi-component events in multichannel seismic data of the HWC DAS and co-located geophone systems. The aim of our study is to investigate whether the use of HWC DAS cable, combined with the novel eco-friendly E-Vibe, can be considered to be an effective monitoring tool in geothermal areas.

In this interdisciplinary study, laboratory results, in particular seismic velocity measurements [4] from Delft University of Technology (TUD) after geological field campaigns at Hellisheiði, were used as an input for the seismic modelling and as a support in the processing of the seismic data. We built a static model using the scarce information available for the larger area [22] and our own laboratory measurements results on samples from the particular area we study [4,23]. By using the results from the field seismic data, and after a joint analysis with the laboratory results, the seismic model was updated to provide synthetic seismograms as a support for the events interpretation in field data. This joint analysis helped both the assessment of the shallower formation properties and deeper settings in the reservoir zone and included the subsurface model calibration along the main 2D monitoring line provided by the trenched HWC DAS sensors for the characterisation and the time-lapse reservoir monitoring.

We describe the processing workflow applied to the data acquired in the seismic campaign at Hellisheiði in July 2021. The investigated area covers the surface projection of a fault which has been identified close to the Reykjavìk Energy Geothermal Plant located in Hellisheiði. Multichannel seismic processing of the data, including tomographic inversion, was performed to better characterise the subsurface and improve the velocity model. In addition, a benchmark among the seismic responses from the different types of sensors was performed and the different wavefield contents highlighted. Thus, the multidisciplinary features of the studies carried out at Hellisheiði offer an extraordinary opportunity for a joint analysis of the different types of acquired data, aiming at the characterisation of the site and enabling the development of a methodology to improve the efficiency of the monitoring campaigns.

2. Geological Overview

The tectonic and volcanic structures that characterise Iceland derive from its position on the Mid-Atlantic Ridge, a divergent plate boundary, and on a hotspot or a mantle plume. The consequences are the presence of a thick crust and a more complex deformation zone than somewhere else on the ridge [24,25], with thirty active volcanic systems identified within the volcanic zones. They consist of a fissure swarm, a central volcano or both [26]. The different ridge segments, volcanic zones and volcanic systems can be seen on Figure 1a.

The Hellisheiði geothermal field (Figure 1b) is located in the southern part of the Hengill volcanic system (Figure 1a,b) in the southwest of Iceland, close to the city of

Reykjavik. The Hengill volcanic system is constituted by a central volcano and a fissure swarm with a graben structure that extends to the northeast and southwest (e.g., [27–31]), and it is located at the junction of the Reykjanes Volcanic Belt (RVB), the Western Volcanic Zone (WVZ) and the South Iceland Seismic Zone (SISZ) (Figure 1a).

The bedrock in the Hengill volcanic system consists mainly of hyaloclastite (tuffs, breccias and pillow lavas) formed during glacial periods with the presence of intrusive rocks and lavas formed during interglacial periods that flowed downhill [30]. Tholeiitic basalt is the main magma type but more silicic rock can be found within the Hengill central volcano. The central volcano itself is a hyaloclastite massif composed of tuyas and tindars. Volcanic activity in the system during the Holocene is characterised by effusive eruptions on the flanks of the central volcano and on the fissure swarm. The two last eruptions occurred 1900 and 5800 years ago [32].

The Hengill area extends over an area of about 112 km^2 and it is one of the largest geothermal areas in Iceland [33,34]. The geothermal activity is also present on the surface as extensive thermal alteration that correlates with faults and fissures [30]. The Hellisheiði geothermal field has a temperature higher than 300 °C at a depth of 1000 m below sea level [35] and the steam combined heat and power plant is one of the biggest in the world with an installed production capacity of 303 MWe and 210 MWth of energy.

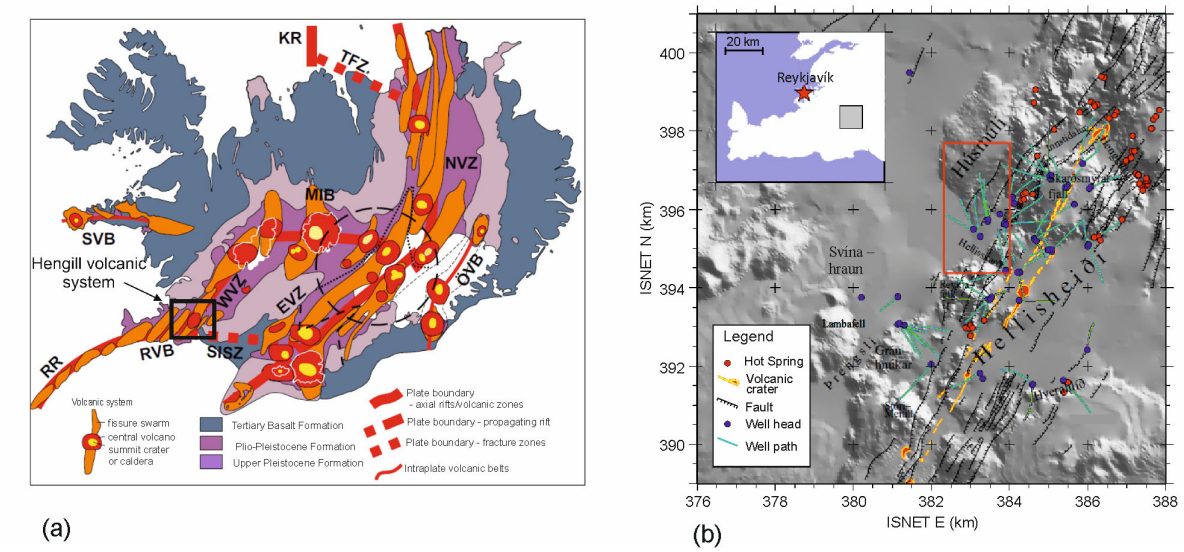

Figure 1. (**a**) Active volcanic systems among volcanic zones and belts in Iceland (after [36]). Abbreviations are as follows: RR, Reykjanes Ridge; RVB, Reykjanes Volcanic Belt; SISZ, South Iceland Seismic Zone; WVZ, West Volcanic Zone; MIB, Mid-Iceland Belt; EVZ, East Volcanic Zone; NVZ, North Volcanic Zone; TFZ, Tjörnes Fracture Zone; KR, Kolbeinsey Ridge; ÖVB, Öræfi Volcanic Belt; and SVB, Snæfellsnes Volcanic Belt. The black dashed circle shows the approximate centre of the Iceland mantle plume/anomaly (after [37]). (**b**) Location map of the Hellisheiði Geothermal Field. The red rectangle indicates the survey acquisition area shown in Figure 2 (modified after [35]).

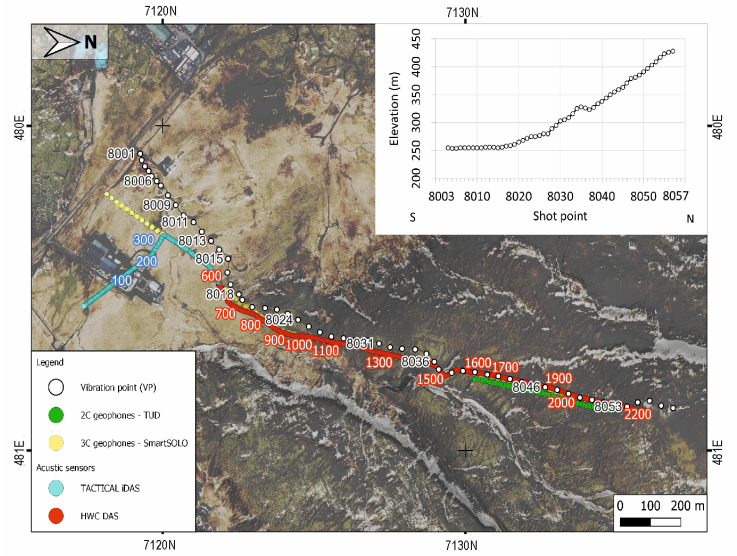

Figure 2. Surface seismic monitoring layout. Line/geometry overview (2C TUD geophones are 20 m down-shifted for display purposes only). The topographic profile of the shot point line is shown in the top-right corner. The map coordinate system is WGS 84/UTM zone 27 N in km.

3. Materials and Methods

This work combines multidisciplinary methods, including laboratory experiments [38], 2D elastic full-waveform seismic modelling, fieldwork to collect reference rock samples, seismic data acquisition and data processing for seismic monitoring of CO_2 injection, as a key geophysical tool to investigate subsurface structural settings and conditions. Active-source acoustic transmission measurements have been performed at field-representative stress conditions in the laboratory [4,38] to estimate the seismic response characteristics of the reservoir formations present at Hellisheiði. Seismic reference velocity models were created along the 2D acquisition line [4]. The seismic properties of the lithological units were estimated initially from average values available in the literature and updated with the laboratory values. Seismic models were used as input for the simulation of 2D seismic wave propagation to define a subsurface model representing the project site. The seismic simulation results were used to design the source–receiver configuration, determine and optimise the operational parameters for the field acquisition and support the QC interpretation and validation of the seismic-monitoring survey results. Early on, the wave-propagation simulation was useful to support the initial analysis of field data. After the QC and the production phase, the acquired data were formatted for processing, including tomographic inversion to improve the built velocity model and multichannel seismic processing to better characterise the site at depth. For the arrangement of the data from the different systems and for the pre-processing, we used proprietary software and a database developed by OGS. The seismic processing was performed using open-source Seismic Unix software (CWPROOT 44R0) and Vista® SLB commercial software 2023.

3.1. Active-Source Seismic Acquisition

The area we investigate in this study covers the surface projection of a fault close to the Reykjavìk Energy Geothermal Plant in Hellisheiði. There are two main targets: the first one aims at monitoring the injected CO_2 in the basaltic rocks of the volcanic system at 700 m depth, while the second one is the deeper target of basaltic rocks from a depth of about 2 km, where the injected CO_2 is expected to migrate to. The design of the receivers and sources acquisition lines was carried out while considering the complex surface logistics, topographic and access conditions. Due to the surface (environmental and topographic)

constraints, the main 2D seismic line was nearly parallel to the interpreted faults system (Figure 2).

The active source is the STORM-10 E-Vibe developed for the purpose of the project by Seismic Mechatronics and operated in vertical mode during this survey. The E-Vibe is an electrically powered seismic source for seismic acquisition, free from the negative aspects of any traditional Vibroseis truck, such as the unwanted vibrations induced by the motor during operations, the higher maintenance costs, higher power consumption and subsequent pollution. The STORM-10 used in this survey weighs 1000 kg, and it operates 10 KN of peak force in the frequency range of 3.6–240 Hz (full drive). The only concern during operations is to keep an appropriate duty cycle that allows the batteries to recharge properly. In this case, a safe duty cycle of 25% was used, resulting in 45 s of recharge after every 15 s of operation. The highly repeatable signals and low internal harmonic distortion result in an environmentally friendly, high-quality active seismic source.

The parameters for the source sweeps were decided after evaluating the initial QC results in the field, by the analysis of the S/N in relation to the number of stacks per shooting point, to set the spacing of the vibration points (VPs), while also considering the operational resources available for the field campaign. The VPs follow the path of the approximately 2 km long trenched linear tactical and HWC DAS fibre-optic cable (Figure 2). The cable used in Hellisheiði has a pitch angle of 30 degrees (i.e., wrapping angle of 60 degrees), 25 mm diameter and was buried at a depth of about 70 cm. Supported by the Reykjavìk Energy partners, the DAS cable was installed by Silixa and is suitable for passive- and active-source monitoring [14,39,40]. The choice of using the HWC cable for active data acquisition aims to improve the broadside sensitivity to P-waves [19], since the standard DAS cable is sensitive mainly to longitudinal strain. In fact, the active-source seismic target was to detect the compressional (P) wavefields expected to emerge with near-vertical travel paths from deep structures and to provide possible information on shear (S) components. In the framework of the active-source seismic campaign, the configuration focused on the recognition of the reflected P- and S-waves for the investigation of the deeper formations. Moreover, the active-source data obtained with the same setting used for the passive seismic survey [14,39,40] were successfully used for velocity analysis purposes via inversion of the first-arrival times of the signals travelling with slant travel paths in the shallow layers.

Simultaneous recording was carried out using co-located geophones (Figure 2), with multi-component sensors deployed for auxiliary signal analysis, enhanced monitoring and QC based on prompt data interpretation, assisted by remote support from headquarters in relevant time. We used two different types of sensors. One line of 92 SmartSolo® 3C (SmartSolo Inc., Calgary, Canada) geophones spaced 20 m apart was installed along the entire 1500 m length of the HWC fibre-optic cable. A second, shorter line (470 m), consisted of 48 10-Hz 2C geophones (hereafter called TUD), recording the vertical and in-line horizontal components, at 10 m intervals.

3.2. On-Field Operations and Remote QC

The remote QC of the acquired data was carried out in near-real-time, enabling rapid decisions on acquisition parameters with the aim of optimising resources. QC included the choice of source vibration parameters: VP interval, number of stacks per VP, sweep-mode frequencies and length, which were tuned during the survey based on the sweep and seismic results of the sample tests conducted at the start of the survey. For this purpose, Seismic Mechatronics provided the source pilot signals. Cross-correlations of the data with the pilot traces were computed and then stacked vertically for QC purposes to provide interpretable data during the field operations. This process, including data conversion, usually took several hours due to the large amount of data from the HWC DAS, which was densely sampled both in space and time (one optical receiver per metre and a sample rate of 1 ms). Figure 3 shows an example of a pilot signal QC for one record of the

vibration point 8041, which enables monitoring of the source performance and highlighting of any problems during the source vibration.

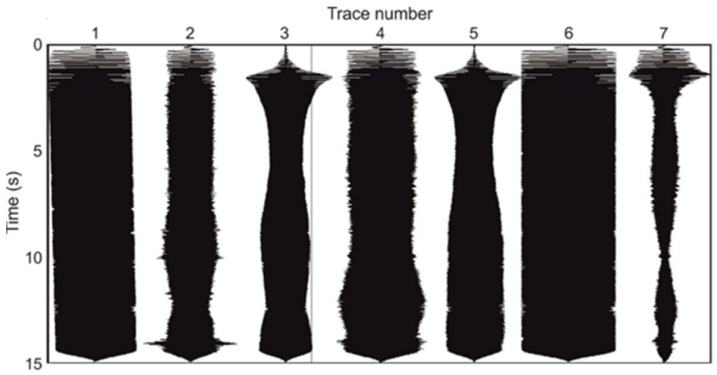

Figure 3. Example of a pilot signal QC. The traces from left to right represent the recorded measured reference (trace 1 in the figure), first recorded reaction mass (acceleration, trace 2), first recorded baseplate (acceleration, trace 3), second recorded reaction mass (acceleration, trace 4), second recorded baseplate (acceleration, trace 5), the external reference (trace 6) and the calculated ground force (trace 7) as a weighted sum of the reaction mass and baseplate values for a selected vibration.

The remote QC was focused on validating the preliminary field seismic results by evaluating the frequency spectrum of the signals, the quality of the pilot signals and the quality of the correlated data (seismic response and overall S/N).

During the QC phase, only the data from the HWC DAS and the TUD geophones were used because the data from the SmartSolo® stations were self-stored and not available in real-time. Therefore, we could compare the SmartSolo® data with the HWC DAS and the TUD data only after the end of the acquisition in order to highlight their similarity and/or the difference in sensitivity in wavefield recording. The signal analysis confirmed the good consistency of the data from different types of sensors [21]. As an example of the consistency of the data, taking into account the different spatial density of the receivers, Figure 4 shows (a) the in-line horizontal component of SmartSolo® geophones, (b) their vertical component and (c) the HWC DAS signal for the vibration position 8041. The HWC fibre does not separately record the Z and horizontal in-line events, but they combine in the recording [21].

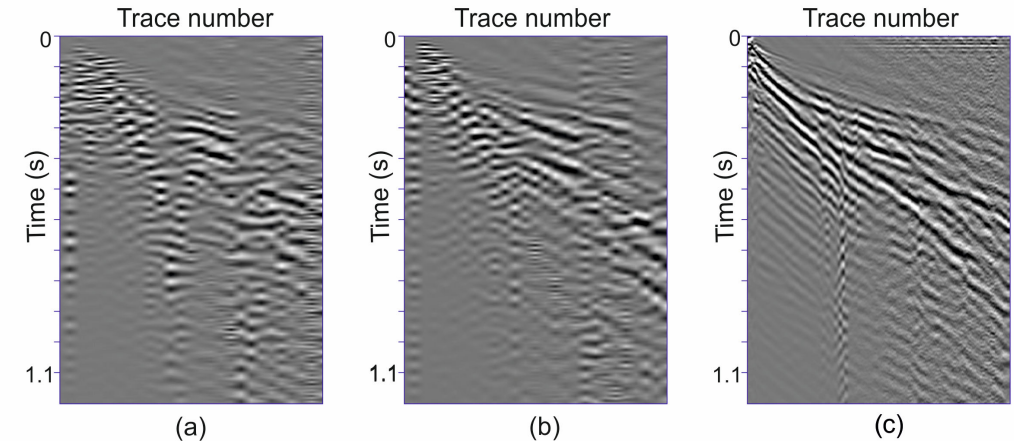

Figure 4. (**a**) In-line horizontal component of SmartSolo® geophones, (**b**) their vertical component and (**c**) the HWC DAS signal for the vibration point 8041.

The production parameters, selected as the results of the in-field and remote QC are described below.

Recording parameters. The seismic source was operated for the production survey by Seismic Mechatronics in P-wave mode, i.e., it vibrated vertically. The source spacing during production was 40 m and stacked 16 times per VP. The sweep of the E-Vibe was 15 s long, sampled at 4000 μs, with a frequency range from 2 to 150 Hz and a start cosine taper of 0.3 s and an end taper of 0.6 s. The record length for DAS, TUD and SmartSolo® was of 20 s, with a sampling rate of 1000 μs, 500 μs and 1000 μs, respectively.

Real-time on-line data. HWC DAS data were acquired on the entire cable length using the Silixa iDAS system and shot data were provided in SEGY format. TUD were acquired using the GEODE system. The output is a standard SEGY file with the collection of the entire daily records.

Deferred-time memory data. Memory data from the SmartSolo® geophones were retrieved only after acquisition, downloaded from the stations' memory and then formatted and analysed at the office.

The seismic campaign produced a large amount of data: 59 VPs, 16 stacks per VP in the production phase, and 944 records of 20 s each for a total of 4225 Mega-traces, corresponding to 770 GB of data.

3.3. Numerical Modelling

We calculated synthetic seismograms for feasibility studies prior to acquisition to evaluate and plan the acquisition parameters such as source geometry and spatial sampling, with the aim of supporting the seismic monitoring campaign with active and passive sources in the area under investigation. Synthetic simulations during and after baseline acquisition were computed to provide data to support QC and to help the field data analysis. The velocity model was updated step by step with the new incoming information from laboratory analysis, tomographic inversion and seismic velocities from processing.

We performed the seismic elastic wavefield modelling with fourth-order in space and second-order in time using a two-dimensional finite-difference scheme based on a staggered grid formulation (modified after [41]). We started with an initial 2D model roughly designed along the DAS and SmartSolo® acquisition lines using a stratigraphic section close to the seismic line [4]. The model—4 km long and 3 km deep—was discretised with square pixels of 2 m on each side. After the acquisition, the initial geological model provided by TU Delft was georeferenced with higher accuracy and the topography was updated according to the elevation of the sources and receivers (Figure 5).

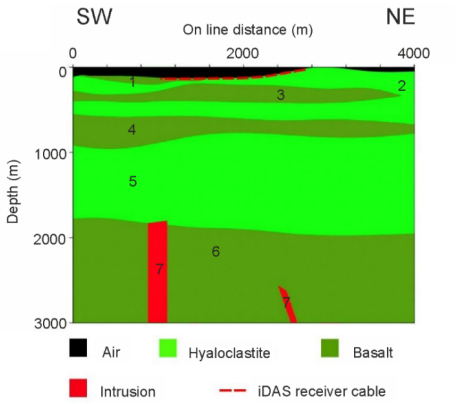

Lithological Units		Velocity
1	Basalt	2415 m/s
2	Hyaloclastite	1768 m/s
3	Basalt	2600 m/s
4	Basalt	2975 m/s
5	Hyaloclastite	1820 m/s
6	Basalt	4830 m/s
7	Hyaloclastite	4430 m/s

Figure 5. Hellisheiði field site geological model used for seismic simulations where the topography was updated according to the elevation of the receivers. The main lithologies are indicated in the legend and the receiver cable position is marked with a red dashed line. The table lists the average velocities for the layers.

To study the wavefields propagating in the subsurface, we simulated data using a vertical and a horizontal point source excited by a Ricker wavelet with a peak frequency

of 20 Hz. We recorded both the synthetic vertical and the horizontal particle velocity components.

During the different phases of the analysis, we tested several seismic models, changing the seismic properties of the layers. In the earlier stage, we used a model with average P-wave velocities (Vp) assigned to each lithology according to their depth (e.g., [18–20]); the density was calculated using Gardener's relationship [42]. S-wave velocity (V_S) was derived using a V_P/V_S ratio of 1.8, an average value estimated using the 1D P- and S-wave velocity profiles calculated during the Control SEISmicity and Manage Induced earthQuakes (COSEISMIQ) Project [43]. This value is in agreement with results reported in the literature for this area (e.g., [42–45]). We updated the P-wave velocity model by comparison of the field and synthetic data. Refs. [4,38] presented the results of elastic laboratory experiments performed on several rock samples from various fresh outcrops in the area around the Hellisheiði geothermal site, including hyaloclastites, dikes/intrusions and basalts with varying porosities. The velocity model was further calibrated using the seismic velocities from these laboratory experiments and the results of the tomographic inversion of the first arrivals (Figure 6). Figure 6a shows the final P-wave velocity model updated with the tomographic results and estimated properties from the laboratory measurements. Figure 6b shows the S-wave velocity model updated with the laboratory results [4] and Figure 6c shows the model with superimposed tomographic results, which highlight a high-velocity body approximately in the position of the first buried basaltic layer. Figure 7 shows the comparison between the horizontal (Y) and vertical (Z) components of the SmartSolo® data for common-shot gathers 8050 and 8041 and the corresponding synthetic particle velocity components computed on the velocity model in Figure 6a using a vertical point source. The comparison between synthetic seismograms and the field data had the aim to cross-validate the laboratory results. This comparison shows a better agreement of synthetic and real data than the previous synthetic simulations based on velocities from the literature (e.g., [44,46,47]). In fact, Figure 7 shows qualitatively similar trends of selected events (e.g., first arrivals and possible reflections), as indicated by the dotted lines in the vertical component of the shots.

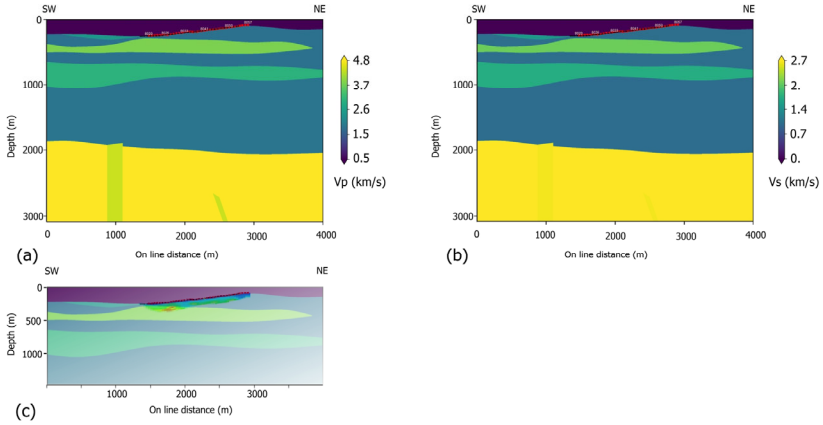

Figure 6. SW-NE-oriented models: (**a**) final compressional velocity model; (**b**) shear velocity model updated using the results from the laboratory transmission experiments. (**c**) A blow-up of the shallower part of the model (up to about 1500 m depth) in (**a**) with the superimposed result of the first-break tomography. The velocity scale is the same as in (a), but a transparency has been applied to highlight the superimposed result.

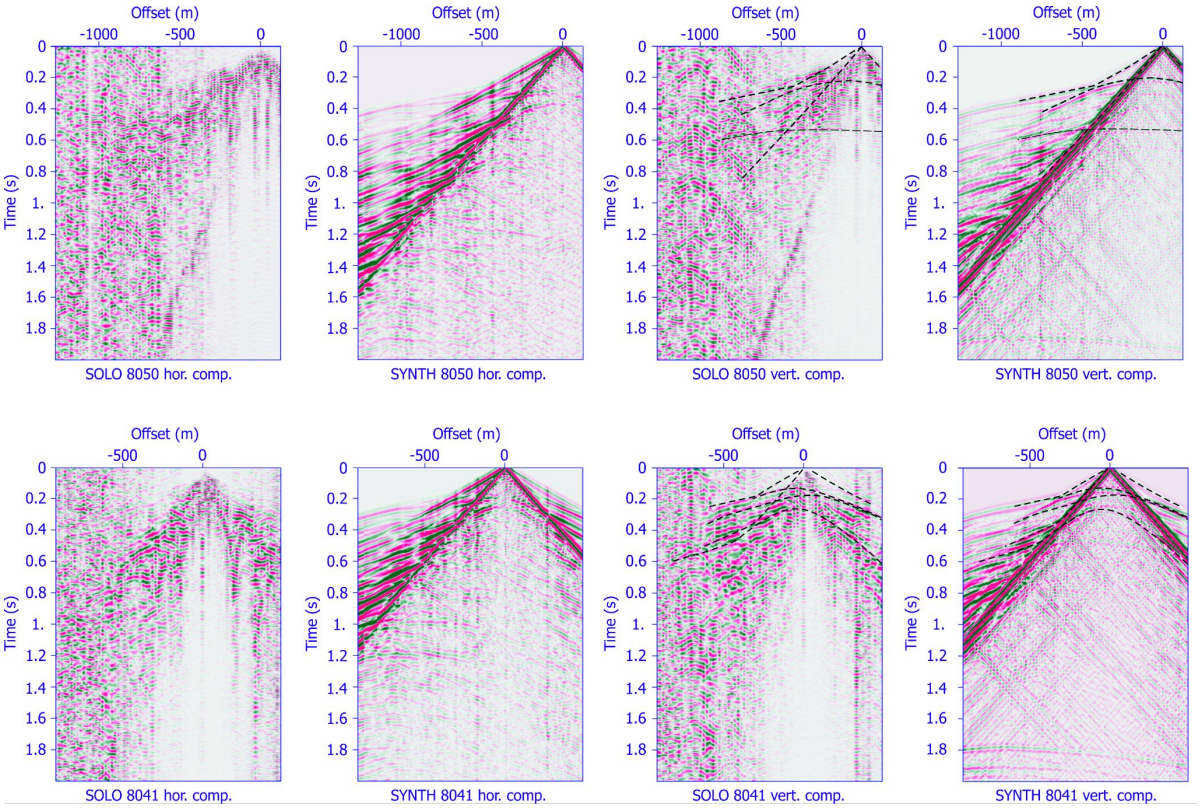

Figure 7. Common-shot gathers: comparison between the horizontal and vertical components of the SmartSolo® geophones and the corresponding synthetic particle velocity components for shots 8050 (**top**) and 8041 (**bottom**). Synthetic data are computed using the velocity models of Figure 6a and a vertical point source with a 20 Hz peak frequency. As an example, the dotted lines in the vertical components of the shots highlight the qualitative similar trends of selected events.

3.4. Signal Pre-Processing

The HWC DAS data present variable levels of S/N; moreover, coherent noise events were identified; therefore, before proceeding with further signal analysis and multichannel data processing of the 2D seismic line, some pre-processing steps were applied to improve the S/N of the HWC DAS data.

The inspection of the field data showed that the HWC DAS dataset was affected by optical noise through the whole shot records. This noise is interpreted as being originated by the optical fibre system itself. This kind of noise consists of horizontal stripes of correlated noise in the correlated data (Figure 8a) that sometimes severely mask the seismic signal, and they are also at shorter offsets. The coherent feature of the noise and its constant amplitude allowed us to develop a tool and analysis procedure to successfully clean the signals and improve the S/N (Figure 8b). This tool performs the estimation and subtraction of the noise. The optical noise in the raw HWC DAS data (i.e., before correlation and stacking) was estimated by selecting a section strongly affected by noise for each record. The common-shot stacking of these noisy traces provides a representative trace of optical noise for the entire gather. This trace can be replicated by building a noise gather which is subtracted from the corresponding HWC DAS original gather. The cleaned raw data are then correlated with the corresponding noise-free pilot signals, i.e., the vibrator sweep, and stacked for the same VP.

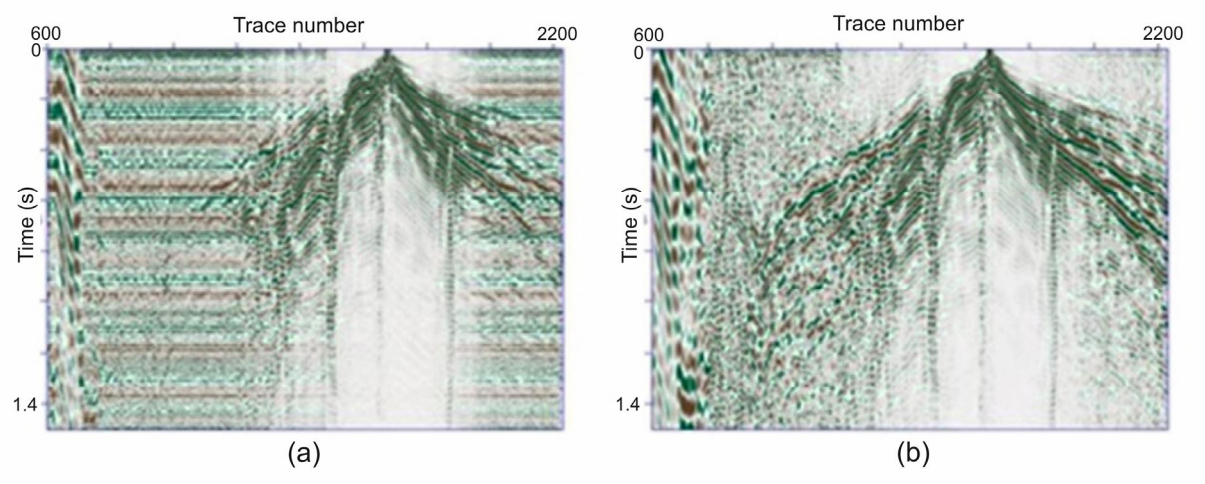

Figure 8. (**a**) Common-shot gather 8041 from HWC DAS recordings affected by optical noise (horizontal stripes). (**b**) The same shot gather after optical noise removal and signal recovery. Data are not filtered.

3.5. Shallow Seismic Signal Inversion

Achievement of high-quality seismic data in a volcanic environment can prove extremely difficult. This limitation is not new, and in spite of significant operational efforts, conventional seismic reflection techniques commonly deliver poor quality data because of diffraction and scattering, attenuation and static problems [48]. For example, the assumption of laterally homogeneous media used in standard velocity analysis fails in onshore volcanic areas, causing degradation of common midpoint (CMP) stacking and inaccurate background velocity models for migration techniques (e.g., [49]). Previous research has concluded that the poor quality of most seismic reflection images within and beneath basalts can be attributed to reverberations caused by the large contrast in the elastic properties of the interbedded clay and basalt [50].

The main goal of the acquisition and processing of the HWC DAS, SmartSolo® and TUD data was to obtain detailed geophysical information about the subsoil of the complex basaltic study area and to demonstrate the feasibility and application of the DAS technologies for the monitoring campaigns. The acquisition with three types of sensors gave us the opportunity to compare the results from different acquisition methods and to validate the results from the new HWC DAS tool (Silixa Ltd., London, UK) with those of the well-known geophones. The dense spatial sampling of the HWC DAS along the main line provides suitable data for tomographic inversion of the first breaks. The analysis used a high number of HWC DAS traces recorded with an optical gauge length of 10 m and a spatial sampling of 1 m. In fact, the HWC DAS traces were suitable for refined signal analysis, while the geophone traces were available with less dense spacing. The inversion results of the picked first arrivals were obtained using the CAT3D OGS software program and provide velocity information and imaging of the shallower formations that were used to build the final model, as shown in Figure 6, and to calculate the static corrections for sources and receivers. The tomographic method is based on a ray tracing algorithm [51] for the direct model and the iterative method SIRT (simultaneous iterative reconstruction technique) [52] for the travel time inversion. A model optimisation technique based on the staggered grid method was also used in the first break tomography. By summing multiple tomographic solutions obtained from a well-conditioned (low null space) base grid shifted in the X and Y directions, the resolution of the final inversion model is increased while the reliability of the tomographic solution corresponding to the base grid is maintained. The resolution of the final tomographic models is 33 m in the horizontal direction, starting from a base grid of 100 m and from 12 to 20 m in depth.

After the inversion, the reliability of the tomographic solution was checked by analysing the time residuals (difference between the observed time and the time calculated on the final model). The RMS value of the residuals was about 5% with respect to the observed times, corresponding to about 6 ms, while the averaged velocity residuals computed on the model pixels was about +/− 50 m/s.

The main results are shown in Figure 9.

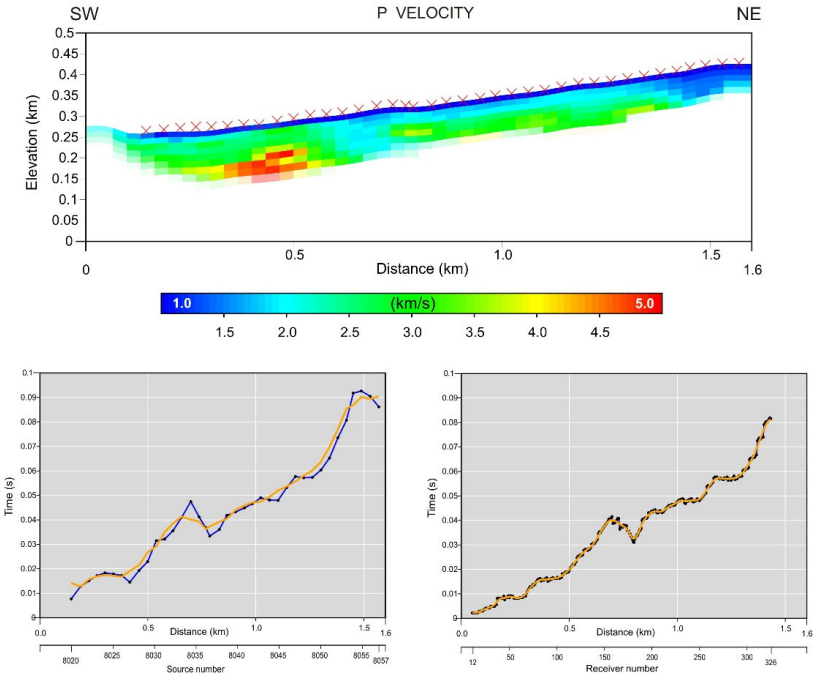

Figure 9. Compressional velocity section obtained from inversion of first arrivals (top), using the simultaneous iterative reconstruction technique (SIRT) algorithm [52]. Red crosses are the shot points. The bottom panels show the smoothed applied static corrections (yellow solid line) and punctual static corrections (blue) for sources (left) and receivers (right), respectively.

3.6. 2D Reflection Seismic Processing

Below, we describe the processing of the HWC DAS, SmartSolo® and TUD surface seismic reflection. The results, their comparison and the discussion of the outcomes are provided in the next section.

Apart from the initial processing dedicated to S/N improvement, the three datasets were processed using the same multichannel processing flow for a more reliable comparison of the results. However, some steps, like trace editing and noise removal, were calibrated to the specific characteristics of the survey. Since the southernmost common-shot gathers are strongly noisy, we considered only the VPs from 8020 to 8057 for HWC DAS and SmartSolo® datasets. Because the TUD line has a shorter extension than the other two lines, as shown in Figure 2, we selected only the VP positions from 8038 to 8053 to ensure adequate CMP fold in the TUD dataset. The resulting maximum fold coverage of the HWC DAS, SmartSolo® and TUD lines is 44, 22 and 14, respectively.

The HWC DAS signal was spatially sampled with a 1 m trace interval, with 1605 traces per VP. The single traces of each VP gather presented large amplitude variations versus offset. To fix them, we individually pre-processed each VP gather. First, we normalised the dataset by dividing the traces amplitudes by the RMS values calculated on the entire gather. To strengthen the signals in the shots, we simulate a pattern of geophones via a weighted moving average. The dense array of receivers provided by the HWC DAS allows simulation of the geophone arrays in this survey by mixing, after a

certain number of S/N trials, an adequate number of traces estimated in 45 traces using a tapered array. Finally, we applied a time exponential power of 1 to recover the spherical divergence in the seismic signals at higher times (Figure 10).

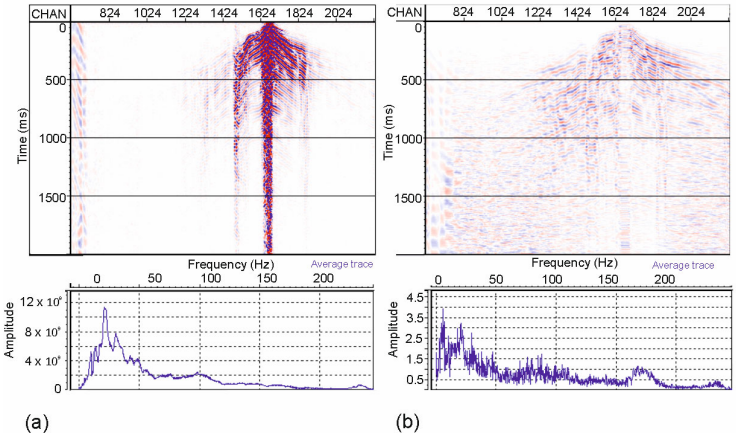

Figure 10. HWC DAS gather (top) for the common-shot gather 8041 before (**a**) and after (**b**) balancing. The blue lines in the bottom of the figures are the corresponding frequency spectra.

Once the amplitudes in the common-shot gathers were balanced and recovered, the first step of the processing was to define the geometry of the line by designing a crooked line that smoothed the acquired 2D line, with a CMP spacing of 5 m. We decided to apply a wider CMP spacing with respect to the 50 cm that should be used for a trace interval of 1 m to make the final stacked section more comparable with the SmartSolo® stacked section, which has a CMP interval of 10 m, and the TUD section with a CPM interval of 5 m.

The static elevation corrections are required to correct the difference in the arrival times due to the relevant variation in the topography (up to 150 m; see Figure 2) and in the velocity of the shallow layers. To obtain the static values at each geophone and VP position, we used the interval shallow velocities obtained from the tomographic inversion of the first-break picking (Figure 9).

Before CMP stacking, we applied an exponential gain correction to compensate for the signal attenuation and absorption in the subsoil, which is high in this volcanic environment [53]. A band-pass filter (5-16-60-70 Hz) was used to reduce the noise components of the signals.

We applied pre-stack predictive deconvolution, using an operator length of 400 ms with the second zero crossing of the autocorrelation as prediction lag, and then repeated the same band-pass filter. The next step was velocity analysis, which is also one of the crucial points in seismic data processing, especially in volcanic environments. Through the combined analysis of the constant velocity stacks (CVS) and the semblance analysis applied to CMP gathers, we obtained a stacking velocity profile (Figure 11) versus time that was used to calculate the normal moveout (NMO) corrections in the CMP gathers and obtain the time-stacked sections (see Section 4), although the low S/N and high absorption by the subsurface lithology made the identification of the stacking velocities non-trivial. The HWC DAS velocities displayed in Figure 11 turned out to be the most reliable, compared to the velocities obtained from SmartSolo® and TUD data, in terms of better coherence in the velocity spectra, probably due to the higher spatial density of sensors of HWC DAS. For this reason, we used these velocities for the NMO correction of the three datasets we processed.

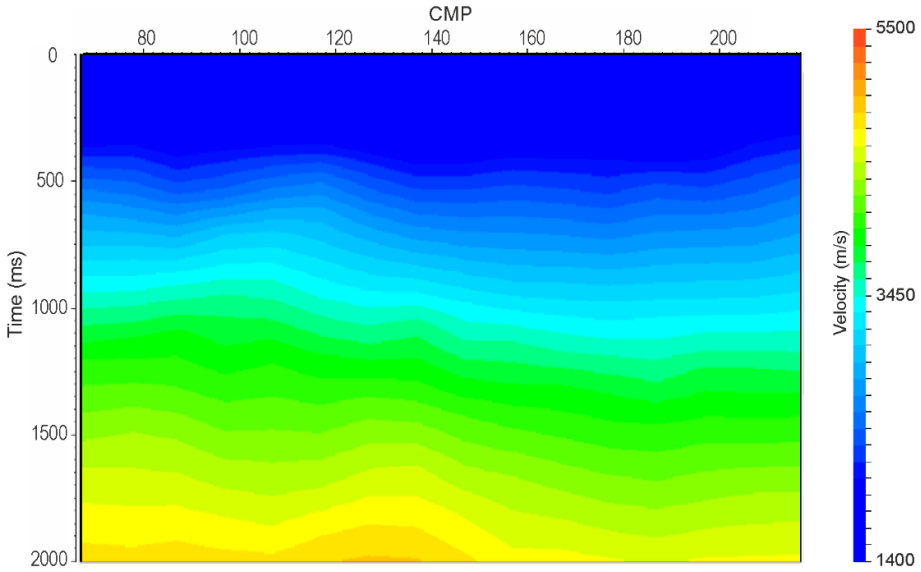

Figure 11. 2D stacking velocity section calculated from the HWC DAS dataset.

The SmartSolo® data presented the similar high-amplitude values and variability as those seen in the DAS dataset. To compensate for differences due to the different acquisition system and number of channels, we applied an ad hoc balancing to the common-shot gathers in the pre-processing phase. We balanced the amplitude values in the common-shot gather data by applying a time power gain and an RMS balancing (Figure 12). The geometry of the line resulted in 143 CMPs spaced at 10 m, since the geophone spacing was 20 m, with a maximum fold coverage of 22.

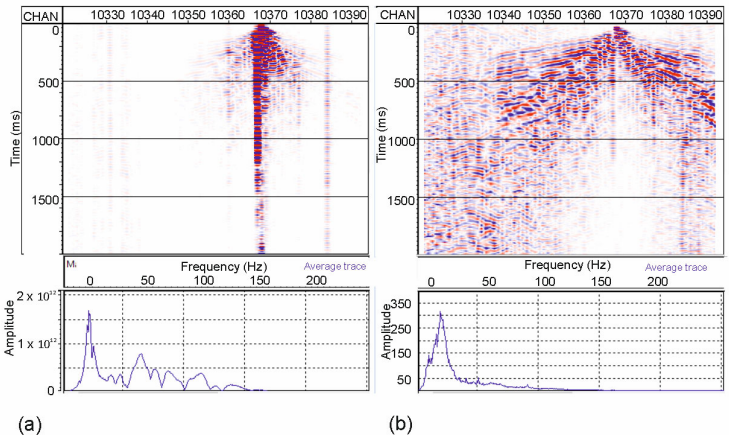

Figure 12. SmartSolo®s common-shot (top) for the common-shot gather 8041 before (**a**) and after (**b**) balancing. The blue lines in the bottom of the figures are the corresponding frequency spectra.

The elevation static-correction values to be applied at each geophone position were calculated using the tomographic velocity model from the HWC DAS dataset (see Figure 9). The static-correction values for the source positions are the same as used for the HWC DAS data. After balancing, the dataset still contained some spikes, i.e., traces with high amplitude, which we have removed shot-by-shot using an automated de-spiking tool. Also, in this case, we ran specific editing to reduce or remove other noise components from the data, e.g., the air wave. The next steps of the processing sequence were the same as used for the HWC DAS dataset (i.e., band-pass filter, predictive deconvolution and stacking), with the same processing parameters and velocity section (Figure 11).

The TUD line presented the high amplitudes seen in the SmartSolo® dataset; therefore, we used the same pre-processing steps to recover and balance the seismic signal (Figure 13). Then, we applied the processing previously described for HWC DAS and SmartSolo® data. Results are discussed in the next section.

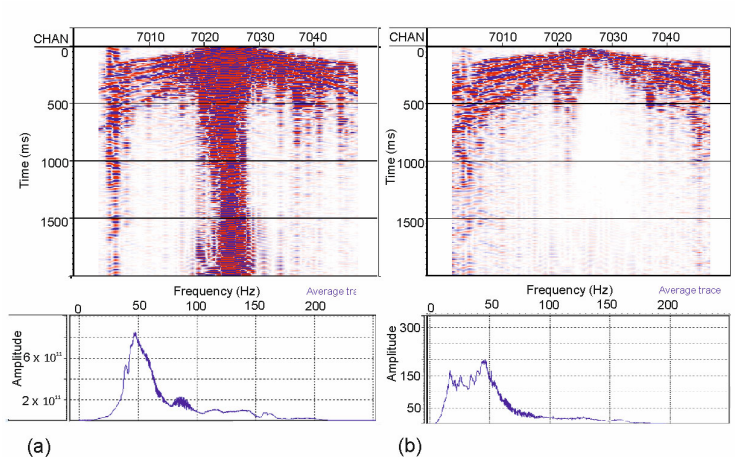

Figure 13. TUD common-shot gather (top) for the common-shot gather 8046 before (**a**) and after (**b**) balancing. The blue lines in the bottom of the figures are the corresponding frequency spectra.

4. Results and Discussion

The project aimed to develop and use innovative seismic monitoring techniques and hardware tools for CCUS purposes. To successfully accomplish the monitoring with an innovative and continuous E-Vibe source together with HWC DAS, the acquisition layout was carefully designed and planned, according to the environmental conditions and site logistic restrictions. The fibre-optic HWC DAS cable configuration was selected for its broadside sensitivity to record up-going signals, enabling detection of the variations in the P-wave reflection coefficients possibly caused by the fluid replacement, and its monitor targeting. The results have shown the effectiveness of the HWC DAS to record subvertical up-going reflections from deep horizons, as shown in Figure 14 where deep reflections are observable up to 1600–1800 ms TWT. The stacked result obtained with the HWC DAS data was band-pass filtered, keeping mainly the lower frequencies (5-16-45-50 Hz) to better highlight the reflectors and boosted by applying a weighted mix among the traces (0.6,1,1,1,0.6). An automatic gain control (AGC) of 500 ms was applied for display purposes only. Reflected events shown by green arrows are observable between 500 and 700 ms TWT and at about 1300–1500 ms TWT (Figure 14), which tentatively represent the reservoirs under investigation. The final stacked time section obtained using the SmartSolo® data is shown in Figure 15 after application of AGC of 500 ms for display purposes only. The final stacked time section obtained using the TUD data is shown in Figure 16 after application of AGC of 500 ms for display purposes only.

The different lateral coverage is clearly visible in the time stacked sections from the three different acquisitions (Figures 14–16) while showing a good agreement for the same reflected events. Despite the complex environment, some reflected energy is visible at about 300–400 ms two-way travel time (TWT), between 500 and 700 ms TWT and at about 1300–1500 ms TWT. In agreement with [40], who analysed passive seismic data, the layers between 700 ms TWT and 1450 ms TWT are identified as the reservoir level where we expect the injected CO_2 (after the baseline survey) to be stored. The geothermal power plant is working and there are several injection and production wells operating on the reservoir, which is known. Consequently, notwithstanding the poor quality of the active surface seismic data, this tentative interpretation is consistent with the location of the reservoir, after a rough time–depth conversion has been computed (not shown in this paper).

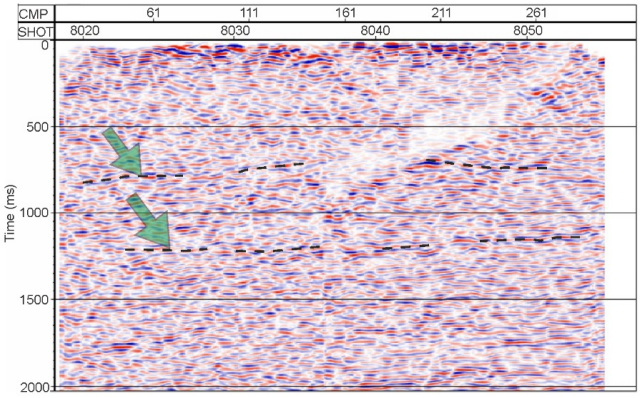

Figure 14. Band-pass-filtered (5-16-45-50 Hz) HWC DAS stacked time section after post-stack mix and AGC for visualisation purposes only. The green arrows and the dashed lines indicate the expected reservoirs in two-way travel time (TWT).

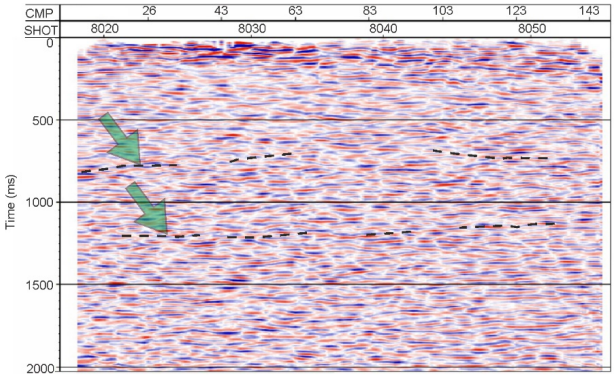

Figure 15. Band-pass-filtered (5-16-45-50 Hz) stacked time section, with post-stack mix and AGC for visualisation purposes, of the SmartSolo® data (vertical component). The green arrows and the dashed lines indicate the expected reservoirs in two-way travel time.

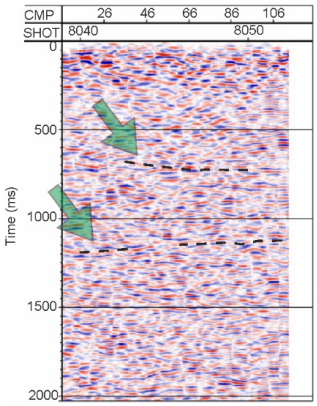

Figure 16. Band-pass-filtered (5-16-45-50 Hz) stacked time section, with post-stack mix of the TUD data (vertical component) and AGC for visualisation purposes. The green arrows and the dashed lines indicate the expected reservoirs in two-way travel time.

The joint use of the auxiliary traditional surface sensors (SmartSolo® and TUD geophones) provided precious data to validate the new HWC DAS technology for monitoring purposes, showing the consistency of the HWC DAS recording signals with those of the multicomponent geophones. The benchmarking among the three stacked sections, taking

into account that the TUD stacked section covers a shorter path, shows a good consistency of the same reflected events. A great advantage of the fibre-optic line is to provide, besides permanent installations of easy deployment useful for monitoring purposes, a dense array of receivers, spaced here with an inter-trace distance of 1 m, with gauge length of 10 m, which allows simulation of geophone arrays in the survey by mixing an adequate number of traces estimated, in this case, at 45.

To obtain useful information from the stacked sections (Figures 14–16) required a processing flow capable of improving the S/N and to attenuate the strong optical and coherent noise. We developed a tool, based both on estimation and subtraction of the noise, to successfully clean the signals from optical noise and improve the S/N (Figure 8b). After array simulation, we improved the data quality to process the data, carry out the velocity analysis and obtain the time stacked section of Figure 14 for the DAS data.

For the shallow formations analysis, the comparison between the velocities from tomographic inversions, obtained using the HWC DAS gathers cleaned from the optical noise, and the seismic model updated with the laboratory results highlights an area of high velocity (Figure 9) where a shallow basaltic body has a P-wave velocity higher than the one from laboratory measurements. One reason for this higher velocity might be the heterogeneities of the basalts. In addition, the shallow hyaloclastite unit also seems to exhibit higher velocities than the values from the laboratory measurements.

The geological model assumes that a relevant part of reservoir rocks in the studied area are basalts and basaltic hyaloclastites. Laboratory results [4] reveal that basalt porosity ranges between 22% and 51%, reflecting different depths within the subsurface, while hyaloclastite and intrusion porosities were measured to be around 47% and 9%, respectively. According to [54], the basaltic hyaloclastites are highly permeable due to their clastic and very porous structure. Permeability can range between 1×10^{-3} mD and $6.4 \times 10^{+3}$ mD. Moreover, the petrophysical analysis shows extremely variable density and P-wave velocity values. The density ranges from 1.2 to 2.34 g/cm^3 and the P-wave velocity ranges from 900 to 4050 m/s. A previous petrophysical study in Southern Iceland provided a classification of the Hjörleifshöfði hyaloclastite sequence [55]. The petrophysical and seismic properties of the basalts are also highly variable; therefore, it would be beneficial to have further data, for example from borehole geophysics, to calibrate and interpret the acquired reflection seismic data and to better characterise the reservoir and the faith of injected CO_2.

As a second phase of the project, the same acquisition was repeated in June 2022 (time-lapse survey) using only the HWC DAS. The repeatability of the baseline and the time-lapse surveys is of key importance in the acquisition phase; therefore, efforts were made in repeating, as precisely as possible, the base acquisition survey parameters and conditions. The aim of the time-lapse survey was to detect seismic differences that can be referred to the migration of the CO_2 in the reservoir. Other targets for future work are the investigation of the different wavefields in the DAS signals (acting as strain rate sensors) and in the geophone signals (acting as velocity transducers), as well as an accurate depth conversion of the time sections. These sections, according to the velocity profile in Figure 10, are provisionally estimated to range between the surface and depths greater than 2 km.

The work on the time-lapse survey is still ongoing and the processing of the time lapse data is outside the scope of this paper.

5. Conclusions

This study presents the baseline active seismic acquisition using an innovative electric source (E-Vibe) and a helically wound cable (HWC) distributed acoustic sensing (DAS) system, and the data processing for seismic imaging and monitoring purposes for CO_2 re-injection at the Hellisheiði geothermal field in Iceland, in the framework of the SUCCEED project. To successfully accomplish the monitoring with an innovative E-Vibe source together with HWC DAS and auxiliary surface sensors (geophones), the acquisition layout was carefully designed and planned according to the environmental

conditions and site logistics restrictions. The main HWC DAS line, used also for passive monitoring purposes, was deployed by burying in a trench dug along an existing hillside path. The fibre-optic HWC DAS configuration was selected for its broadside sensitivity to record up-going signals, enabling detection of the variations in the P-wave reflection coefficients caused by the fluid replacement, which is the target of the monitoring. The active source E-Vibe acquisition was performed in the vertical vibration mode along the same line path of the HWC DAS. The great advantage of the fibre-optic line is to provide, besides permanent installations of easy deployment, a dense array of receivers spaced in this survey with an inter-trace distance of 1 m, with gauge length of 10 m. In the baseline survey accomplished in July 2021, a network of co-located geophones was used to characterise the HWC DAS seismic response via analytic comparison with multicomponent geophone recordings. Signals from two geophone types were acquired alongside the HWC DAS, 10-Hz 2C geophones and 3C SmartSolo® geophones. The comparison showed good consistency between the different datasets: between HWC DAS and geophones and between geophones. The analysis has shown that the HWC DAS data contain wavefields observable both in the vertical and horizontal components, thus confirming that HWC DAS records both P-wave and S-wave signals, as well as converted waves, making them suitable for monitoring purposes of deep reservoirs. The results obtained from the three stacked sections from the different types of sensors highlight the same reflection zones and agree with the results from a passive body-wave survey, where the possible storage level is identified between 700 ms and 1450 ms. The analysis of the shallow formations was performed by tomographic inversion of the first breaks, providing the reconstruction of the velocity model in the shallower layers.

Synthetic modelling was used, starting from the early feasibility-study phase to support the acquisition and, later, during the seismic data processing phase. The synthetic model was integrated from the beginning of the survey activities with results from laboratory transmission measurements on outcrop samples. In the subsequent phases, the modelling was used to tune the velocity fields by comparison with the field common-shot data, and subsequently for time-lapse simulation with the hypothesis of low changes in percentage of the compressional velocity in the porous layer where the fluid substitution was assumed in a preliminary analysis. During the second survey at Hellisheiði, the recording parameters of the first survey were replicated to ensure repeatability for the subsequent time-lapse analysis. The aim of the time-lapse survey is to detect seismic differences that can be related to the migration of the CO_2 in the target formation.

The results of the Hellisheiði surveys indicate that the applied innovative seismic method provides results in accordance with the available information and can provide subsurface information during injection of CO_2 and brine. It could thus be used as an effective characterisation and monitoring tool even when low quality of the surface seismic data would not allow for a detailed characterisation. This study highlighted new and precious insights on the capabilities of HWC DAS and the new E-Vibe in volcanic areas used for geothermal energy production.

Author Contributions: Methodology, C.B., E.B., B.F., F.P., G.B., D.D., M.T.G.J. and A.S.; software, B.F., F.M., G.v.O. and A.S.; validation, F.P.; formal analysis, C.B., E.B. and G.B.; investigation, C.B., E.B., F.P., G.B., D.D., M.T.G.J. and A.S.; resources, G.v.O.; data curation, F.M.; writing—original draft preparation, C.B.; writing—review and editing, C.B., E.B., B.F., F.P., F.M., D.D., A.L.S., A.C., A.S. and S.D.; visualization, C.B., E.B., B.F. and G.B.; supervision, F.P., A.C., A.S. and S.D.; project administration, S.D.; funding acquisition, S.D. All authors have read and agreed to the published version of the manuscript.

Funding: This study was carried out within the framework of SUCCEED, which is funded through the ACT programme (Accelerating CCS Technologies, Project No 294766).

Institutional Review Board Statement: Not applicable.

Informed Consent Statement: Not applicable.

Data Availability Statement: The data that support the findings of this study are available from the corresponding author upon reasonable request.

Acknowledgments: Financial contributions by the Department for Business, Energy and Industrial Strategy UK (BEIS), the Ministry of Economic Affairs and Climate Policy, the Netherlands, the Scientific and Technological Research Council of Turkey (TUBITAK), Orkuveita Reykjavíkur/Reykjavik Energy Iceland (OR) and National Institute of Oceanography and Applied Geophysics—OGS Italy are gratefully acknowledged. The SmartSolo® geophones were provided by courtesy of Swiss Seismological Service (SED) at Eidgenössische Technische Hochschule Zürich (ETH) and Reykjavík Energy (OR). The authors are grateful to Jordan Bos, William Perry, Auke Barnhoorn, Anna Korre, Baldur Brynjarsson, Vala Hjörleifsdóttir, Anne Obermann and Pilar Sánchez-Pastor for their important contributions to the success of the project. The authors acknowledge SLB® who provided the academic Vista® software (2023) licenses to OGS and the creators and developers of the open-source seismic utilities package Seismic Unix, which was supported by the Center for Wave Phenomena (CWP) at the Colorado School of Mines (CSM) and currently it is supported by John Stockwell.

Conflicts of Interest: Author Athena Chalari was employed by the company Silixa Ltd., Anna L. Stork was employed by the company Silixa Ltd., Gijs van Otten was employed by the company Seismic Mechatronics. The remaining authors declare that the research was conducted in the absence of any commercial or financial relationships that could be construed as a potential conflict of interest.

References

1. Lund, J.W.; Huttrer, G.W.; Toth, A.N. Characteristics and Trends in Geothermal Development and Use, 1995 to 2020. *Geothermics* **2022**, *105*, 102522. https://doi.org/10.1016/J.GEOTHERMICS.2022.102522.
2. Durucan, Ş.; Korre, A.; Parlaktuna, M.; Şentürk, E.; Wolf, K.-H.; Chalari, A.; Stork, A.; Nikolov, S.; De Kunder, R.; Sigfússon, B.; et al. SUCCEED: A CO2 Storage and Utilisation Project Aimed at Mitigating against Greenhouse Gas Emissions from Geothermal Power Production. In Proceedings of the 15th International Conference on Greenhouse Gas Control Technologies, GHGT-15; 2021.
3. Parlaktuna, M.; Durucan, Ş.; Parlaktuna, B.; Sinayuç, Ç.; Janssen, M.T.G.; Şentürk, E.; Tonguç, E.; Demircioğlu, Ö.; Poletto, F.; Böhm, G.; et al. Seismic Velocity Characterisation and Survey Design to Assess CO2 Injection Performance at Kızıldere Geothermal Field. Turkish Journal of Earth Sciences **2021**, 30, 1061–1075. https://doi.org/10.3906/YER-2106-22.
4. Janssen, M.; Draganov, D.; Bos, J.; Farina, B.; Barnhoorn, A.; Poletto, F.; Van Otten, G.; Wolf, K.; Durucan, S. Monitoring CO2 Injection into Basaltic Reservoir Formations at the Hellisheiði Geothermal Site in Iceland: Laboratory Experiments. In Proceedings of the 83rd EAGE Annual Conference & Exhibition, Madrid, Spain, 6–9 June 2022; Volume 2022, pp. 1–9. https://doi.org/10.3997/2214-4609.202210474.
5. Ragnheidardottir, E.; Sigurdardottir, H.; Kristjansdottir, H.; Harvey, W. Opportunities and challenges for CarbFix: An evaluation of capacities and costs for the pilot scale mineralization sequestration project at Hellisheidi, Iceland and beyond. *International Journal of Greenhouse Gas Control* **2011**, *5*, 1065–1072.
6. Snæbjörnsdóttir, S.Ó.; Tómasdóttir, S.; Sigfússon, B.; Aradóttir, E.S.; Gunnarsson, G.; Niemi, A.; Basirat, F.; Dessirier, B.; Gislason, S.R.; Oelkers, E.H.; Franzson, H. The geology and hydrology of the CarbFix2 site, SW-Iceland. *Energy Procedia* **2018**, *146*, 146-157.
7. Snæbjörnsdóttir, S.Ó.; Wiese, F.; Fridriksson, T.; Ármansson, H.; Einarsson, G.M.; Gislason, S.R. CO_2 storage potential of basaltic rocks in Iceland and the oceanic ridges. *Energy Procedia* **2014**, *63*, 4585-4600.
8. Alfredsson, H. A.; Hardarson, B. S.; Franzson, H.; Gislason, S. R. CO2 sequestration in basaltic rock at the Hellisheidi site in SW Iceland: stratigraphy and chemical composition of the rocks at the injection site. *Mineralogical Magazine* **2008**, *72(1)*, 1–5.
9. Matter, J.M.; Broecker, W.S.; Gislason, S.R.; Gunnlaugsson, E.; Oelkers, E.H.; Stute, M.; Sigurdardóttir, H.; Stefansson, A.; Alfreõsson, H.A.; Aradóttir, E.S.; et al. The CarbFix Pilot Project–Storing Carbon Dioxide in Basalt. *Energy Procedia* **2011**, *4*, 5579–5585. https://doi.org/10.1016/J.EGYPRO.2011.02.546.
10. Sigfússon, B.; Arnarson, M.P.; Snæbjörnsdóttir, S.Ó.; Karlsdóttir, M.R.; Aradóttir, E.S.; Gunnarsson, I. Reducing Emissions of Carbon Dioxide and Hydrogen Sulphide at Hellisheidi Power Plant in 2014-2017 and the Role of CarbFix in Achieving the 2040 Iceland Climate Goals. *Energy Procedia* **2018**, *146*, 135–145. https://doi.org/10.1016/J.EGYPRO.2018.07.018.
11. Gunnarsson, I.; Aradóttir, E.S.; Oelkers, E.H.; Clark, D.E.; Arnarson, M.Þ.; Sigfússon, B.; Snæbjörnsdóttir, S.; Matter, J.M.; Stute, M.; Júlíusson, B.M.; et al. The Rapid and Cost-Effective Capture and Subsurface Mineral Storage of Carbon and Sulfur at the CarbFix2 Site. *International Journal of Greenhouse Gas Control* **2018**, *79*, 117–126. https://doi.org/10.1016/J.IJGGC.2018.08.014.
12. Gunnarsson, I.; Aradóttir, E.S.; Sigfússon, B.; Gunnlaugsson, E.; Júlíusson, B.M. Geothermal Gas emission from Hellisheiði and Nesjavellir Power Plants, Iceland. *GRC Transactions* **2013**, *37*, 785–790.
13. P Aradóttir, E.S.; Gunnarsson, I.; Sigfússon, B.; Gunnarsson, G.; Júliusson, B.M.; Gunnlaugsson, E.; Sigurdardóttir, H.; Th Arnarson, M.; Sonnenthal, E.; P Aradóttir, E.S.; et al. Toward Cleaner Geothermal Energy Utilization: Capturing and Sequestering

CO_2 and $H2_S$ Emissions from Geothermal Power Plants. *Transp Porous Media* **2015**, *108*, 61–84. https://doi.org/10.1007/s11242-014-0316-5.
14. Stork, A.L.; Poletto, F.; Draganov, D.; Janssen, M.; Hassing, S.; Meneghini, F.; Böhm, G.; David, A.; Farina, B.; Schleifer, A.; et al. Monitoring CO2 Injection with Passive and Active Seismic Surveys: Case Study from the Hellisheiði Geothermal Field, Iceland. In Proceedings of the Proceedings, 16th International Conference on Greenhouse Gas Control Technologies, GHGT-16, Lyon, France, 23-27 October 2022.
15. Mondanos, M.; Coleman, T. Application of Distributed Fibre-Optic Sensing to Geothermal Reservoir Characterization and Monitoring. *First Break* **2019**, *37*, 51–56.
16. Foulger, G. Geothermal Exploration and Reservoir Monitoring Using Earthquakes and the Passive Seismic Method. *Geothermics* **1982**, *11*, 259–268. https://doi.org/10.1016/0375-6505(82)90032-3.
17. Blanck, H.; Jousset, P.; Reinsch, T.; Ryberg, T.; Clarke, A.; Aghayev, R.; Hersir, G.P.; Henninges, J.; Weber, M.H.; Krawczyk, C.M.; et al. Passive Seismic Measurements Using the Distributed Acoustic Sensing (DAS) Technology on the Reykjanes Peninsula, SW-Iceland. *AGUFM* **2019**, *2019*, S41A-01.
18. Willis, M.E. Distributed Acoustic Sensing for Seismic Measurements – What Geophysicists and Engineers Need to Know Society of Exploration Geophysicists: Houston, TX, USA, 2022. https://doi.org/10.1190/1.9781560803850.
19. Kuvshinov, B.N. Interaction of Helically Wound Fibre-Optic Cables with Plane Seismic Waves. *Geophys Prospect* **2016**, *64*, 671–688. https://doi.org/10.1111/1365-2478.12303.
20. Poletto, F.; Finfer, D.; Corubolo, P. Broadside Wavefields in Horizontal Helically-Wound Optical Fiber and Hydrophone Streamer. In Proceedings of the Paper presented at the 2015 SEG Annual Meeting, New Orleans, Louisiana, October 2015.; OnePetro, October 18 2015.
21. Meneghini, F.; Poletto, F.; Bellezza, C.; Farina, B.; Draganov, D.; Van Otten, G.; Stork, A.; Böhm, G.; Schleifer, A.; Janssen, M.; et al. Monitoring CO2 Injection: Feasibility Study and Preliminary Results from a Multi-Tool Active-Seismic Acquisition at the Hellisheiði Basaltic Geothermal Reservoir. *submitted to Acta Geophysica* **2023**.
22. Poux, B.; Gunnarsdóttir, S.H.; O´brien, J. 3-D Modeling of the Hellisheiði Geothermal Field, Iceland, Using Leapfrog. *GRC Transactions* **2018**, *42,* 524-542.
23. Janssen, M.; Russel, J.; Barnhoorn, A.; Draganov, D.; Wolf, K.; Durucan, S. Seismic Velocity Characterization and Modelling for Synergetic Utilisation of CO2 Storage Coupled with Geothermal Energy Extraction. In Proceedings of the 1st Geoscience and Engineering in Energy Transition Conference, GET 2020, Strasbourg, France, 16–18 November 2020; European Association of Geoscientists and Engineers, EAGE: Bunnik, The Netherlands, 2020; Vol. 2020, pp. 1–6.
24. Einarsson, P. Earthquakes and Present-Day Tectonism in Iceland. *Tectonophysics* **1991**, *189*, 261–279. https://doi.org/10.1016/0040-1951(91)90501-I.
25. Einarsson, P. Plate Boundaries, Rifts and Transforms in Iceland. *JÖKULL* **2008**, *58*, 35–58.
26. Thordarson, T.; Höskuldsson, Á. Postglacial Volcanism in Iceland. *JÖKULL* **2008**, *58*, 197–228
27. Sæmundsson, K. *Hengill: Map of Thermal Activity, Alteration and Hydrology [Cartographic Material] 1:25000*; Iceland GeoSurvey: Reykjavík, Iceland, 1995.
28. Saemundsson, K. Vulkanismus Und Tektonik Des Hengill-Gebietes in Südwest-Island. *Acta Naturalia Islandica* **1967**, *2*, 1–105.
29. Sæmundsson, K. *Hengill: Geological Map (Bedrock) [Cartographic Material] 1:5000.*; Iceland GeoSurvey: Reykjavík, Iceland, 1995.
30. Franzson, H.; Gunnlaugsson, E.; Árnason, K.; Saemundsson, K.; Steingrímsson, B.; Harðarson, B.S. The Hengill Geothermal System, Conceptual Model and Thermal Evolution. In Proceedings of the World Geothermal Congress 2010, Bali, Indonesia, 25–29 April 2010; pp. 25–29.
31. Franzson, H.; Kristjánsson, B.R.; Gunnarsson, G.; Björnsson, G.; Hjartarson, A.; Steingrímsson, B.; Gunnlaugsson, E.; Gíslason, G. The Hengill-Hellisheiði Geothermal Field. Development of a Conceptual Geothermal Model. In Proceedings of the World Geothermal Congress 2005, Antalya, Turkey, 24–29 April 2005; pp. 24–29.
32. Sæmundsson, K. Hengill. In *Catalogue of Icelandic Volcanoes*; Ilyinskaya, E., Larsen, G., Gudmundsson, M.T., Eds.; European Geosciences Union: Munich, Germany, 2016.
33. Harðarson, B.S. Geothermal Exploration of the Hengill High-Temperature Field. In Proceedings of the Expanded abstract, Short Course IX on Exploration for Geothermal Resources; UNU-GTP, G. and K., Ed.; at Lake Bogoria and Lake Naivasha, Kenya, 2-3 November 2014.
34. Tómasdóttir, S. Flow Paths in the Húsmúli Zone, Iceland. Master thesis, Uppsala Universitet: Uppsala, Sweden, 2018.
35. Gunnarsson, G. Temperature Dependent Injectivity and Induced Seismicity— Managing Reinjection in the Hellisheiði Field, SW-Iceland. *GRC Transactions* **2013**, *37*, 1020-1025.
36. Jóhannesson, H.; Sæmundsson, K. *Geological Map of Iceland, 1:500.000. Bedrock Geology*; Iceland GeoSurvey: Reykjavík, Iceland, 1998.
37. Wolfe, C.J.; Th Bjarnasont, lngl; VanDecar, J.C.; Solomon, S.C. Seismic Structure of the Iceland Mantle Plume. *Nature* **1997**, *385*, 245–247.
38. Janssen, M.T.G.; Barnhoorn, A.; Draganov, D.; Wolf, K.H.A.A.; Durucan, S. Seismic Velocity Characterisation of Geothermal Reservoir Rocks for CO2 Storage Performance Assessment. *Applied Sciences (Switzerland)* **2021**, *11*, 3641. https://doi.org/10.3390/APP11083641/S1.

39. Stork, A.L.; Chalari, A.; Durucan, S.; Korre, A.; Nikolov, S. Fibre-Optic Monitoring for High-Temperature Carbon Capture, Utilization and Storage (CCUS) Projects at Geothermal Energy Sites. *First Break* **2020**, *38*, 61–67. https://doi.org/10.3997/1365-2397.fb2020075.
40. Hassing, S.H.W.; Draganov, D.; Janssen, M.; Barnhoorn, A.; Wolf, K.-H.A.A.; Van Den Berg, J.; Friebel, M.; Van Otten, G.; Poletto, F.; Bellezza, C.; et al. Imaging CO2 Reinjection into Basalts at the CarbFix2 Reinjection Reservoir (Hellisheiði, Iceland) with Body-Wave Seismic Interferometry. *Geophys. Prospect.* **2023**, https://doi.org/10.1111/1365-2478.13472
41. Levander, A.R. Fourth-Order Finite-Difference P-5V Seismograms. *Geophysics* **1988**, *53*, 1425–1436.
42. Gardner, G.H.F.; Gardner, L.W.; Gregory, A.A.R. Formation Velocity and Density-the Diagnostic Basics for Stratigraphic Traps. *GEOPHYSICS* **1974**, *39*, 770–780. https://doi.org/10.1190/1.1440465.
43. Obermann, A.; Wu, S.M.; Ágústsdóttir, T.; Duran, A.; Diehl, T.; Sánchez-Pastor, P.; Kristjansdóttir, S.; Hjörleifsdóttir, V.; Wiemer, S.; Hersir, G.P. Seismicity and 3-D Body-Wave Velocity Models across the Hengill Geothermal Area, SW Iceland. *Front Earth Sci (Lausanne)* **2022**, *10*, 969836. https://doi.org/10.3389/feart.2022.969836.
44. Tryggvason, A.; Rögnvaldsson, S.T.; Flóvenz, G. Three-Dimensional Imaging of the P-and S-Wave Velocity Structure and Earthquake Locations beneath Southwest Iceland. *Geophys. J. Int* **2002**, *151*, 848–866.
45. Jousset, P.; Haberland, C.; Bauer, K.; Arnason, K.; Weber, M.; Fabriol, H. Seismic Tomography and Long-Period Earthquakes Observation and Modelling at the Hengill Geothermal Volcanic Complex, Iceland. In Proceedings of the World Geothermal Congress 2010, Bali, Indonesia, 25–30 April 2010; p. 7.
46. Bjarnason, I.T.; Menke, W.; Flóvenz Ó.G.; Caress D. Tomographic Image of the Mid-Atlantic Plate Boundary in Southwestern Iceland. *J Geophys Res* **1993**, *98*, 6607–6622. https://doi.org/10.1029/92JB02412.
47. Stefánsson, R.; Böðvarsson, R.; Slunga, R.; Einarsson, P.; Jakobsdóttir, S.; Bungum, H.; Gregersen, S.; Havskov, J.; Hjelme, J.; Korhonen, H. Earthquake Prediction Research in the South Iceland Seismic Zone and the SIL Project. *Bulletin of the Seismological Society of America* **1993**, *83*, 696–716. https://doi.org/10.1785/BSSA0830030696.
48. Dell'Aversana, P.; Ceragioli, E.; Morandi, S.; Zollo, A. A Simultaneous Acquisition Test of High-Density 'Global Offset' Seismic in Complex Geological Settings. *First Break* **2000**, *18*, 87–96. https://doi.org/10.1046/J.1365-2397.2000.00053.X.
49. Jin, S.; Madariagas, R. Nonlinear Velocity Inversion by a Two-Step Monte Carlo Method. *GEOPHYSICS* **1994**, *59*. https://doi.org/10.1190/1.1443618.
50. Pujol, J.; Fuller, B.N.; Smithson, S.B. Interpretation of a Vertical Seismic Profile Conducted in the Columbia Plateau Basalts. *Geophysics* **2012**, *54*, 1258–1266. https://doi.org/10.1190/1.1442585.
51. Böhm, G.; Rossi, G.; Vesnaver, A. Minimum-Time Ray Tracing for 3-D Irregular Grids. *Journal of seismic exploration* **1999**, *8*, 117–131.
52. Stewart, R.R. *Exploration Seismic Tomography*; Society of Exploration Geophysicists, 1991.
53. Shaw, F.; Worthington, M.H.; White, R.S.; Andersen, M.S.; Petersen, U.K.; Group, S. Seismic Attenuation in Faroe Islands Basalts. *Geophys Prospect* **2008**, *56*, 5–20. https://doi.org/10.1111/j.1365-2478.2007.00665.x.
54. Frolova, J.; Ladygin, V.; Franzson, H.; Sigurðsson, O.; Stefánsson, V.; Shustrov, V. Petrophysical Properties of Fresh to Mildly Altered Hyaloclasitie Tuffs. In Proceedings of the Proceedings World Geothermal Congress; 2005, Antalya, Turkey, 24–29 April 2005; pp. 24–29.
55. Greenfield, L.; Millett, J.M.; Howell, J.; Dougal, J.A.; Watton, T.; Healy, D.; Hole, M.J.; Planke, S. The 3D Facies Architecture and Petrophysical Properties of Hyaloclastite Delta Deposits: An Integrated Photogrammetry and Petrophysical Study from Southern Iceland. *Basin Research* **2020**, *32*, 1081–1104. https://doi.org/10.1111/bre.12415.